Friction and Wear of Additive Manufactured Polymers in Dry Contact

F. Dangnan[a*], C. Espejo[a], T. Liskiewicz[b], M. Gester[c], A. Neville[a]

*pm12fd@leeds.ac.uk

[a]*Institute of Functional Surfaces (iFS), School of Mechanical Engineering, University of Leeds, Leeds, LS2 9JT, UK.*
[b]*Manchester Metropolitan University, Faculty of Science and Engineering, Manchester M15 6BH, UK*
[c]*P&G Reading Innovation Centre, 460 Basingstoke Road, Reading, RG2 0QE, UK*

Abstract

The use of additive manufacturing (AM) is widely advancing the scope of rapid prototyping and manufacturing in tribological applications and material science research. However, there is still limited research focused on investigating the frictional and wear performance of AM polymers, especially of Polyjet manufactured parts. This work focuses on the effect of varying the contact load on the friction and wear mechanisms of additively manufactured acrylonitrile butadiene styrene (3D ABS) and Verogray polymers fabricated using Polyjet technology. Loads of 1, 5 and 10 N were applied under dry sliding contact with a 52100 steel counterface at room temperature. Dependence of friction and wear on the surface orientation to the sliding direction is noted. The results demonstrate that at 1 N load, the friction coefficient is primarily dependent on the orientation of the surface to the sliding direction. However, at higher loads of 5 N and 10 N, this dependency is shown to be a function of the bulk material properties rather than the surface roughness. Further correlation between the surface morphology and wear rate is shown to be dependent on the bulk material properties and the applied load. The results from this study provide alternate application uses for Polyjet materials in metal-polymer tribo-contacts for improved friction and wear performance.

Keyword: Additive Manufacturing, Polyjet technology, Friction, Wear, Surface Topography

1. Introduction

Additive manufacturing (AM) is the process of creating objects directly from a computer-aided design (CAD) by adding layer-upon-layer of materials. This technique affords flexibility in manufacturing and provides geometrical stability for varied engineering applications [1]. Currently, one of the most well-established processes for providing detailed and accurate AM parts is the Polyjet 3D photopolymer technique. This technique builds functional prototypes in various grades of high-performance photopolymer materials such as Digital ABS Plus (3D ABS), Vero materials (e.g. Verogray), Tango, Biocompatible MED610 and Durus (i.e. simulated polypropylene) [2]. The Polyjet process builds 3D-modelled parts in a layer-by-layer sequence through reactive polymerization using UV-light [2]. This produces parts with a detailed surface finish, a layer resolution (the minimum layer thickness achieved by a print head in one pass) of ~ 14 µm and accuracy (the dimensional measure of closeness of a 3D printed part to its digital model within a certain XY tolerance) of ~ 0.1 mm [2].

Despite their relatively reduced mechanical and structural properties compared with most metallic and ceramic composites [3], polymer-based materials (PBM) exhibit excellent self-lubricating properties, providing an advantage in tribo-pair applications such as lip seals, rollers, ball bearings and artificial joints [4]. A highly cross-linked PBM is crucial in preventing material loss and fragmentation during surface contact in tribological

application [5]. Nevertheless, the effect of print orientation introduces a new set of challenges when characterising both the friction and wear of these materials. Mohammed *et al.* [6] reported the influence of printing conditions on the tribological behaviour and wear mechanism of fused deposition modelled (FDM) parts. They reported that sliding wear behaviour was significantly affected by raster angle and build orientation. Dawuod *et al.* [7] also claimed that the isotropicity of the wear behaviour of pure ABS depends on the raster angle orientation to the applied load.

The deformation regime under sliding wear presents a time-dependent friction behaviour at the contact [8] and, as such, has shown to be a combination of several factors including system properties or response rather than solely a material property [6, 9]. Additionally, several authors [6, 9, 10] have demonstrated the influence of load and sliding conditions on the deformation and wear for AM polymers in varying applications involving FDM parts. It is, therefore, crucial to understand the performance of Polyjet printed parts in similar applications so that key parameters can be optimised to maintain reliability for industrial use. It is generally accepted that no single polymer performs optimally under certain tribological conditions [10]. It is, therefore, imperative to understand the tribological behaviour of additively manufactured parts under different wear regimes. No previous studies could be found investigating the tribological behaviour of Polyjet materials under varying loading conditions in reciprocating sliding wear.

The functional correlation between process parameters and wear have shown that PBM undergoes several modes of wear, including abrasive, corrosive, fatigue and adhesive wear [11]. The most common mechanism, abrasive wear, is self-evident during a steel-on-polymer tribo contact [8]. Generally, there is no single wear regime involving PBM on steel but a combination of different regimes [12]. In two-body abrasive wear, a harder contacting surface ploughs and micro-cuts through the asperities of the softer surface. On the other hand, three-body abrasive wear involves the synergistic interaction of a third body which acts as an erosive medium on both contacting surfaces. In both cases, adhesive wear junctions are formed during the rubbing and shearing process at the real contact interface, producing micro-size particles. A transfer film is subsequently formed on the counter surface and if stable enough, contributes to a reduction in the coefficient of friction (COF). Due to the direct contact between the transfer film and the polymer material, it acts like two polymer surfaces rubbing against each other in a polymer-on-polymer tribo contact. However, new microparticles are constantly formed and sheared in the process leading to increasing wear rate and a higher coefficient of friction [8].

The frictional response of additively manufactured PBM provides a different dimension to understanding the role material properties such as hardness and surface roughness play in different tribological regimes [13]. Recently, a lot of work has been focused on improving dimensional accuracy [14], material strength characterisation [15, 16] and surface roughness refinement [17], all to improve the tribological behaviour at the contact interface [15, 16]. Dawuod *et al.* [7], noted an increase in the friction behaviour of 3D-printed acrylonitrile butadiene styrene (ABS) parts manufactured by FDM when a positive raster gap was introduced (an increase in the distance between two adjacent filaments, deposited in the same print plane). They subsequently demonstrated that this increase was because of the independent nature of the deposited structure within the filament modelling body contributing to elevating the coefficient of friction. Sood *et al.* [18], in a similar experiment, also reported an increase in the wear rate of 3D printed ABS when a positive gap is used during manufacturing. The use of a positive gap, they noted, encourages the creation of pits on the wear surface.

Past reviews have focused on the optimisation of the process operating parameters such as build orientation, part spacing and surface quality on product functionality (e.g. mechanical properties) [19, 20]. Stansbury *et al.* [21] reported the influence of build orientation on the mechanical isotropicity of Polyjet printed materials. Cazón *et al.* [20] went further to report on the effect that print orientation and post-processing has on Polyjet-printed parts in terms of material strength and surface properties. They further noted that part orientation of the Polyjet material has no significant effect on the ultimate strength but rather the material stiffness and fracture stress. Further tests by Gaya *et al.* [22] showed no significant influence on the mechanical properties when part spacing along the x-axis is used. The highest effect on the relaxation modulus was observed along the y-axis. However, the effect of these parameters on the tribological performance is yet to be adequately explored.

In this study, two Polyjet materials namely, 3D ABS (Digital ABS Plus) and Verogray were chosen because of their wide usage and unique structural properties and stability. The tribological measurements were conducted on both polymers to compare their friction and wear behaviour under dry reciprocating sliding conditions at loads of 1,5 and 10 N. The parallel and perpendicular orientations to the sliding direction was tested to assess the differences in tribological performance for both polymers. Surface morphologies of the worn surfaces have also been discussed. The findings obtained through this study will help in shaping future research into Polyjet material tribology and guide the use of these materials for reciprocating sliding applications in industrial processes.

2. Experimental details

2.1. Material and sample preparation

Polyjet Digital ABS Plus (3D ABS) and Verogray grade polymers were chosen for this study. 3D ABS possesses similar structural and mechanical properties to that of pure ABS and Verogray has excellent durability and strength [2], making both ideal choices for material prototyping. The liquid photopolymer resins (3D ABS and Verogray) were supplied by Stratasys USA. SolidWorks®2018 was used to model the required sample prototypes as the stereolithography files (.stl). The stereolithography files were later exported to the Object®1000 device for printing. A default printer setting of 300, 300 and 1600 dpi (dots per inch) resolution was used for the x, y and z print coordinates respectively. The raster orientation for printing (This is the sequential path taken by the printer nozzle or head to the X-axis of the print bed orientation) was set at 0/90 flat (as shown in Figure 1), which is the unidirectional orientation default print setting. For all samples printed for the tribological and mechanical properties studies, similar default printer settings were used. The surface finish was set to "glossy finish" for all printed parts used in both tribological and mechanical properties studies. For the tribological studies, a 20mm x 15mm x 2mm rectangular-shaped test samples were printed (Figure 1). For the tensile tests, each specimen was modelled according to ASTM D638 for the Typ IV modified dogbone shape with a thickness of 4mm (as seen in Figure 2). After printing, samples were cleaned using a pressurised water-jet station to remove all support material present.
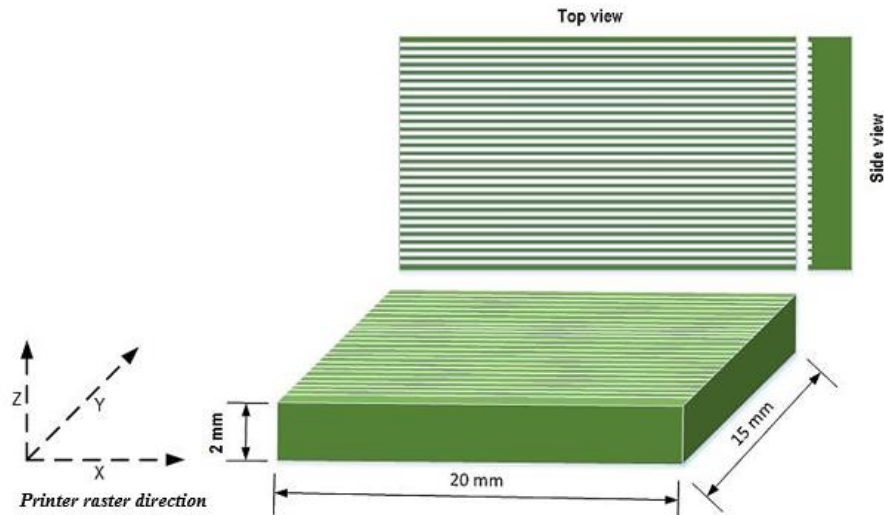
Figure 1. Schematic of the Polyjet printer bed orientations (flat) and raster angle [0/90] investigated in this experiment.
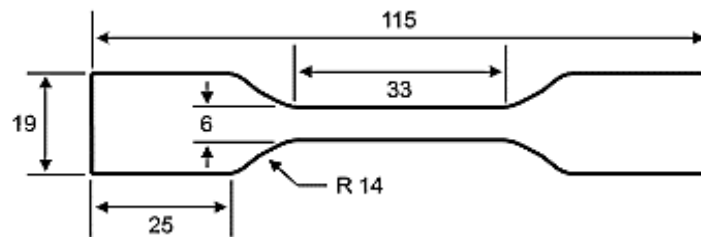

Figure 2. Schematic of the ASTM D638 Type IV tensile specimen. The scale is specified in mm.

2.2. Characterisation of Polyjet printed parts

Several characterisation techniques were implemented in this work to quantify the physical, mechanical and chemical properties of the additively manufactured polymers. The surface roughness in the parallel and perpendicular directions was measured with a 2D contact Talysurf PG1800 profilometry scanner with a tip radius of 2 µm. A defined scan length of 4.7 mm with a Gaussian filter cut-off of 2.5 mm and a bandwidth of 100:1 was utilised. Measurement direction (Figure 3) for both parallel and perpendicular orientations were defined as X_1-X_2 and Y_1-Y_2 respectively. To characterise the tensile behaviour of the polymers, experimental testing using geometries specification outlined in ASTM D638 for the Type IV was used. Tensile testing of each specimen was conducted on the INSTRON 5967 universal tensile machine equipped with a 30kN load cell. The INSTRON wedged grips were displaced at a rate of 5 mm/min with a data (force, strain and grip displacement) capture rate of 100Hz. An axial clip-on 2630-107 extensometer (25mm gauge length) was used to measure strain. To ensure reliable and repeatable data, the tensile tests were repeated three times and an average was calculated. The wear mechanisms and surface deformation after tribological testing was imaged using a Hitachi SU8230 Scanning Electron Microscope (SEM). A Perkin Elmer Paragon 1000 FTIR was used to characterise the chemical structure of the polymer samples.

2.3. Friction and Wear test

The friction and wear tests were evaluated using a Bruker Universal Material Test (UMT) Tribo Lab with the linear reciprocating module in a ball-on-plate configuration under dry sliding conditions. The test rig consists of a lower reciprocating linear drive which houses the sample holder assembly, a variable speed motor with a maximum speed of 10 mm/s and an upper assembly unit which consists of a ball sample holder rigidly attached to a pivoted loading cell. Both upper and lower samples were secured using their respective sample holders to prevent them from moving during testing. The upper specimen (ball) was made of 52100 hardened steel with a measured surface roughness (R_a) of 0.07 µm (using a similar technique as described in section 2.2), a hardness of 65 HRC [23] and diameter of 6.5 mm. The room temperature was maintained at 23 ± 2 °C throughout testing. Before the tribological tests, all samples (3D ABS, Verogray and 52100 Steel) were thoroughly cleaned with ethanol to rid the surfaces of all impurities. The maximum sliding speed was 8 mm/s and the test time was 60 minutes. The applied normal loads were kept constant at 1, 5 and 10 N throughout the respective tests with a sliding distance of 2 mm. The tangential force, normal load, coefficient of friction and linear velocity were monitored and recorded throughout the test cycle. The data capture rate was set at 10Hz throughout the entire test duration. All friction data presented in this study are an average of three repeats. The maximum Hertzian contact pressures (P_{max}) (Table 1) are calculated using the expression given in Equations 1-3 for the contact between a rigid sphere and a flat surface [24].

$$P_{max} = \frac{3W}{2\pi a^2} \qquad (1)$$

Where W is the applied normal load, a is the contact radius given by the expression:

$$a = \left[3\frac{WR}{8E^*}\right]^{\frac{1}{3}} \qquad (2)$$

Where R is the ball radius and E^* is the equivalent Young's modulus at the contact given by:

$$\frac{1}{E^*} = \frac{1-v_1^2}{E_1} + \frac{1-v_2^2}{E_2} \qquad (3)$$

Where v_1 and v_2 are the Poisson's ratio of the 52100-steel ball (0.29) and 3D printed specimen respectively. For the 3D ABS and Verogray, Poisson's ratios of 0.36 and 0.4 were used respectively. E_1 and E_2 are the Young's moduli for both 52100 steel ball and 3D printed specimen (Table 3). A Young's modulus of 205 GPa was used for the 52100 steel. All data regarding the mechanical properties of the 52100-steel ball was provided by the supplier.

Table 1. Maximum contact pressure at each of the loads tested.

Applied Load (N)	Sample	P_{max} (MPa)
1	3D ABS	33
	Verogray	36
5	3D ABS	57
	Verogray	62
10	3D ABS	71
	Verogray	78

Mass loss due to wear (ΔM) is given by Equation 4, which is the difference between the initial mass (M_1) and final mass (M_2) [25, 26]. Materials that exhibit higher resistance to wear will have lower volume and mass loss [26]. All test specimens were weighed before and after the experiment using a single pan Mettler Toledo XPR205 analytical balance with a 0.01mg readability. To accurately compute ΔM, each measurement was taken as the mean of three repeats.

$$\Delta M = (M_1 - M_2) \qquad (4)$$

The specific wear rate S_W of the test specimen is given as:

$$S_W = \frac{\Delta V}{F_N x\ S_d} \qquad (5)$$

Where F_N is the normal applied load (N), S_d is the total sliding distance (m) and (ΔV) is the volume loss (m^3).

3. Results and Discussion

3.1. Surface Roughness Profile

Figure 3 presents a typical surface roughness profile for both parallel and perpendicular orientations for the 3D printed polymers studied. For the parallel orientation, the surface profile scan shows consistent periodicity for the peak height surface topography. However, at 90° orientation (perpendicular) the profile shows varying peak height values for the scan length with fairly consistent periodicity between the consecutive peaks. similarly. It was observed further that the differences in measured heights of asperities in the parallel and perpendicular scans are seen to affect the measured R_a values. Arnold *et al.* [27] noted that, for surfaces showing higher accuracy along with a parallel orientation, the R_a value is always lower, because the measurement section runs seamlessly along the sample edge. This is shown in Table 2 with the parallel scan on both samples showing a lower R_a value when compared to their respective perpendicular scans. It is also noted that Verogray has a lower parallel scan roughness whereas 3D ABS has a lower perpendicular scan roughness.
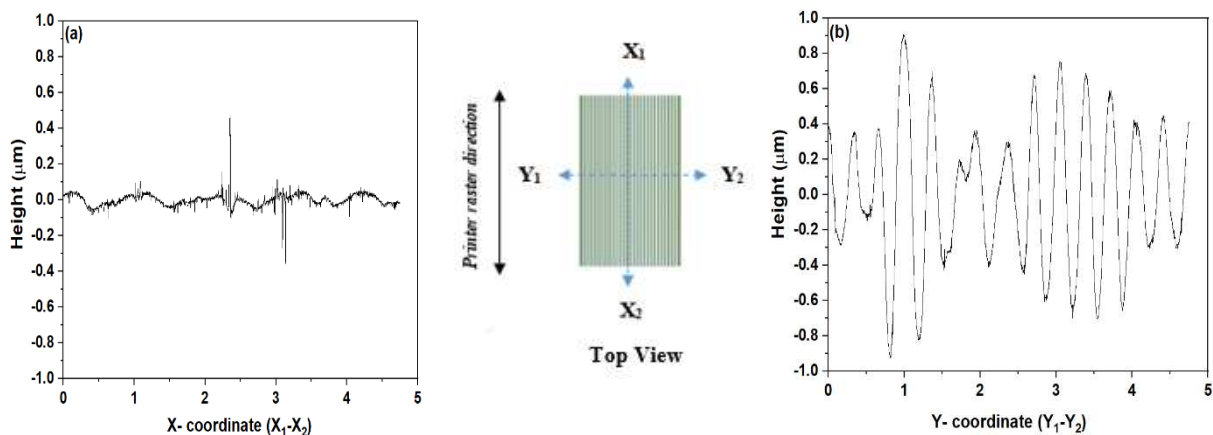

Figure 3. Surface roughness profile for print orientation of (a) parallel and (b) perpendicular to print orientation.

Table 2. R_a values for both orientations for the test specimen.

Specimen	R_a (μm)	
	Parallel	Perpendicular
3D ABS	0.083 ± 0.030	0.440 ± 0.090
Verogray	0.026 ± 0.030	0.580 ± 0.080

3.2. Tensile testing

The Elastic Modulus and Tensile Stress at Yield for 3D ABS and Verogray are shown in Table 3. Although 3D ABS showed the lowest Elastic Modulus, no significant differences are seen between both specimens. A similar trend for the Tensile Stress at Yield for both specimens is observed. For the majority of 3D printed parts studied in the literature [7, 19], mechanical properties variation has been primarily linked to the build direction [19]. Contrary to other 3D manufacturing types such as FDM and selective laser sintering (SLS), where significant part-to-part variation is dependent on the local disparity in the process conditions (raster orientation, airgap, trajectory and bed levelling of the printer), any deviation of these conditions results in varying mechanical properties [19]. In this work, the effect of varying key process parameters such as the speed of print, raster spacing and orientation were not explored as most of the literature show no or minimal mechanical anisotropy during testing [14, 21].

Table 3. Mechanical properties of 3D ABS and Verogray.

Specimen	Mechanical Properties	
	Elastic Modulus (GPa)	Tensile Stress at Yield (GPa)
3D ABS	1.23 ± 0.06	0.0530 ± 0.0001
Verogray	1.35 ± 0.04	0.0460 ± 0.0040

3.3. Fourier transform infrared spectroscopy

The infrared (IR) spectra for each of the 3D printed polymers are shown in Figure 4 where selected IR peaks are displayed to confirm their polymer structure [28] are highlighted. For both IR spectra bands, an O-H absorption peak which occurs at wavenumbers 3550 – 3200 cm^{-1} showing a characteristic large singlet transmittance peak is observed in both polymers [29]. For the Verogray sample, this peak is seen to have a stronger transmittance in comparison with the 3D ABS polymer which may be attributed to the high affinity of the polymer surface to adsorbed H_2O molecules when exposed to the atmosphere after printing. Aside from the distinguishable O-H infrared peak observed for both polymers, comparable IR vibration patterns were seen from wavenumbers 3000 – 1500 cm^{-1}. Between the major IR vibration bands is the sp^3– CH stretching observed between 3000 – 2800 cm^{-1} wavenumbers, which is characteristic of aliphatic compounds [30]. Further, the IR transmission bands detected between 2000 – 1500 cm^{-1} are due to C=O and C=C stretching, with C=C occurring around 1650cm^{-1} due to its weak absorption properties [29].
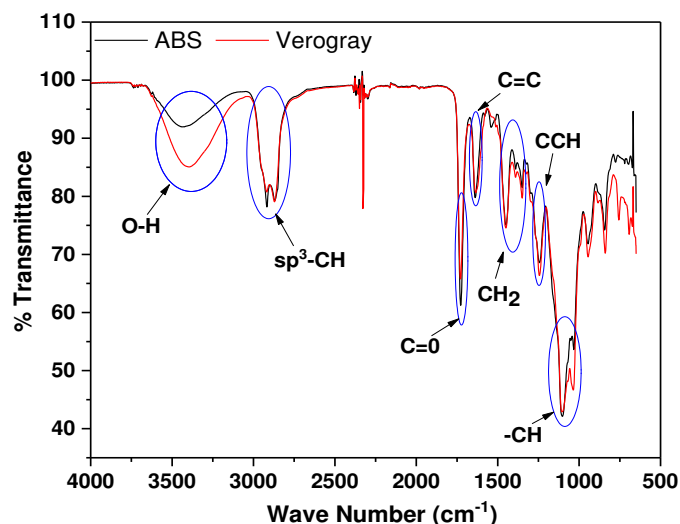
Figure 4. FTIR spectrum plot for Polyjet printed 3D ABS and Verogray specimen.

3.4. Time frictional behaviour response

The time-dependent frictional response for 3D ABS and Verogray at 1, 5 and 10 N loads are shown in Figure 5.

There were distinguishable differences observed in the coefficient of friction (COF) response amongst the different loads, orientation and specimen studied. As shown in Figure 5, the friction coefficient for both test specimens showed an obvious running-in period for both orientations followed by a steady-state regime. 3D ABS is noted to have a more pronounced running-in period. The friction force initially increases rapidly as a result of irregular contact between the sample surface and test specimen. A steady-state is reached after more conformal contact is achieved. It can be noted that the surface asperities contribute significantly to the initial spike in the COF value as the surface deforms plastically [18, 31]. Recent work by Wang *et al.* [10] provides similar evidence in support of this phenomenon for PTFE, PR, UHMWPE, and PEEK at a constant load of 10N. For the two orientations (parallel and perpendicular) tested, the effect of surface anisotropy on the COF is evident as the perpendicular orientation is seen to promote higher COF values under 1N load for both specimens.

It is a common phenomenon in polymer tribology to see a directly proportional relationship between frictional force and applied load as define by Amontons's law of friction [32]. Nevertheless, at certain loads, this proportionality breaks down [8]. At 1N load, it is shown that the COF evolution with time (Figure 5 (c) and (d)) for Verogray produced the characteristic delayed pattern followed by a sudden spike in the COF value before achieving steady-state. This phenomenon is highly pronounced within the first 10 minutes of the test when the sliding orientation is perpendicular to the raster direction (Figure 5 (d)). At moderate loads of 0.02 to 1 N, Rees [33] noted that the friction coefficient decreases with increasing load due to elastic deformation of the surface asperities. However, Myshkin *et al.* [8] explained that contrary to the elastic deformation theory, there is also the existence of a plastic deformation regime where the COF increases with increasing load. Kragelskii [34] further demonstrated that at higher loads (>1 N), the friction coefficient passes the minimum elastic deformation point into the plastic zone where the friction coefficient increases with increasing applied load.
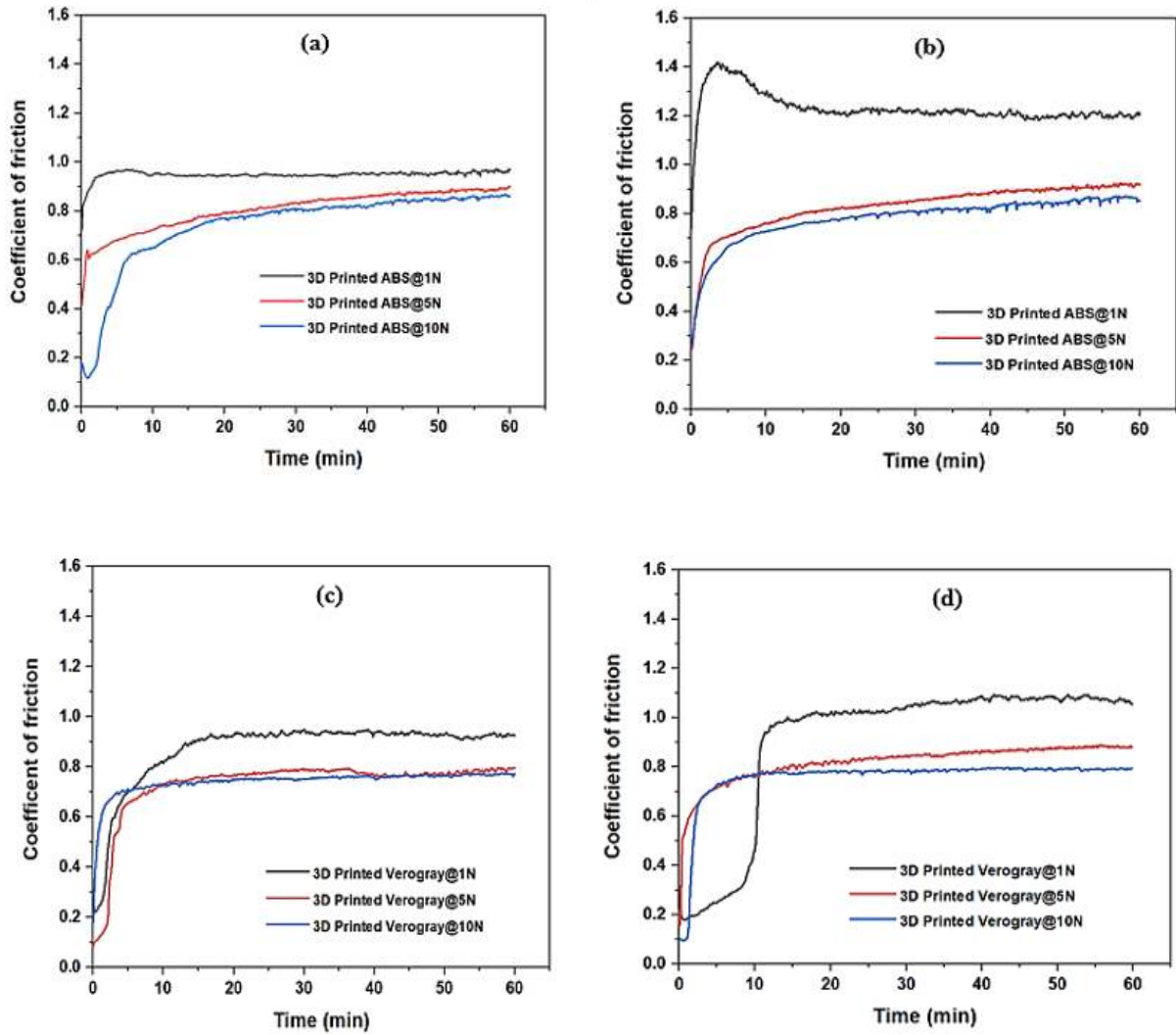
Figure 5. Variation of friction coefficient under varying contact load and sliding orientation for 3D ABS (a) parallel (b) perpendicular, and Verogray (c) parallel (d) perpendicular.

At higher applied loads (5 N and 10 N), the COF is seen to be lower across the time range in both orientations. After achieving steady-state, the COF is seen to be independent of the specimen orientation but rather on the bulk material properties. Quaglini and Dubini [35] observed that resistant to deformation during sliding in PBM is highly related to material modulus and yield stress at high contact pressure where plastic deformation is dominant. Hence, an increase in the surface ploughing resistance due to bulk material properties such as modulus and yield stress would further contribute to the friction force increase as exhibited by the 3D ABS test specimen.

The average steady-state COF values (reached after 20 mins of testing) are shown in Figure 6. The highest COF is observed when the test specimen is oriented perpendicular to the sliding direction at 1N load. For the 3D ABS, the COF value reaches 1.20, whereas, for the Verogray, the value reduces to 0.93. Even though lower COF values were reached under 1N loads for the parallel orientation for both specimens, similar trends were observed in both 3D ABS and Verogray. The lowest COF value of 0.76 was reached under the 5N load for Verogray in the parallel orientation. The experimental results suggest that changing the surface orientation to the sliding direction and applied load can alter the coefficient of friction of the additively manufactured polymers. This behaviour is

consistent with the adhesion theory of friction, where the resistance to shear during sliding is affine to the relationship between the contact area and shear stress [36].
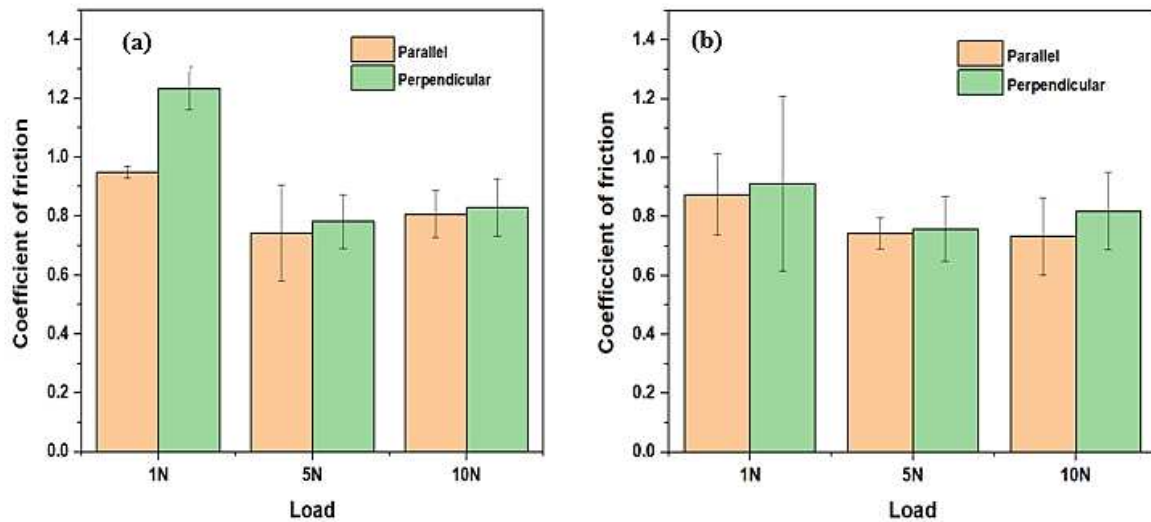

Figure 6. Average coefficient of friction plot in steady-state for (a) 3D ABS (b) Verogray.

3.5. Transient tribological response

To further understand the transient behaviour observed under 1 N load for the test specimens under both orientations, a comprehensive study to correlate friction performance and wear mechanisms is performed. By comparing the frictional response for Verogray and 3D ABS with maximum testing time of 10 minutes with wear images at 2, 6 and 10 minutes, different tribological responses are observed under reciprocating sliding wear. Figure 7 (a) and (b) show the friction and wear response for the 3D ABS under both parallel and perpendicular orientations respectively. Under the perpendicular orientation, it is observed that the friction coefficient increases steadily until it reaches a maximum value of ~1.4 after which it stabilised. Micrograph images of the worn surface show progressing severity of the deformation of the asperities with sliding time. At 2 minutes, the initiation of surface microcracks perpendicular to the sliding direction and the extensive abrasive deformation of the surface asperities are observed, which are continuous to the end of the test. As the compressive load is maintained at the contact surface due to the reciprocating sliding, fatiguing occurs, causing the initiation and development of microcracks. Fukahori and Yamazaki [37] in the study of abrasion pattern formation in natural rubber vulcanizate, observed similar abrasive pattern followed by a series of parallel micro ridges perpendicular to the sliding direction. They attributed this to micro-vibration of the contact surface induced by periodic bumping of the adhered surface during sliding. Consequently, the resulting frictional force is increased by increasing the real contact area between the surface asperities resulting in a larger friction coefficient value of ~1.4 for the perpendicular print orientation. For the parallel orientation as seen in Figure 7 (a), similar running in periods are observed at the start of the test but stabilised at a lower COF value of ~ 0.9 as compared with the perpendicular orientation. SEM imaging shows predominantly abrasive wear damage at 2 minutes on the 3D ABS surface followed by similar perpendicular microcracks. However, the main observable difference is the generation and containment of wear debris within the wear track which acts as a lubricating film to control friction.

The transient friction and wear response of the Verogray specimen are shown in Figure 7 (c) and (d) for both parallel and perpendicular orientations respectively. Under the parallel orientation, the COF is seen to suddenly drop after the start of the test followed by a period of stabilising friction in the steady-state period. Corresponding SEM analysis of the surface shows evidence of debris containment within the wear track which acts as a third body within the tribological system, thus forming a low shear-strength interfacial film that acts as a lubricant to promote lower friction values at this stage. However, the COF value after 2 minutes is seen to steadily increase to a maximum value of 0.72 at 10 minutes of testing. Corresponding SEM images of the wear transition from an initial low COF value to a maximum value shows progressively increasing debris generation that is not contained within the tribological contact but continuously displaced away from the contact, promoting excessive wear. Boparai et al. [38] in the study of the tribological behaviour of Nylon6-Al-Al$_2$O$_3$ and 3D printed ABS from FDM method, also demonstrated the effect of material wear properties on friction which changes over time with different applied loads. Similarly, for the perpendicular orientation, an initial increase in the friction coefficient is observed followed by a sudden drop. This low friction regime is further followed up by a progressively delayed running-in period reaching a COF value of 0.42 at 10 minutes. SEM images show severe deformation of the asperities, promoting the generation of wear debris (2 minutes). The wear debris is further dislodged and contained within the micro-channels present on the contact surface, creating an effective lubricating film in the process to reduce friction at extended testing times. After 10 minutes, the generation of micro-cracks and layer detachment promotes an increase in friction.
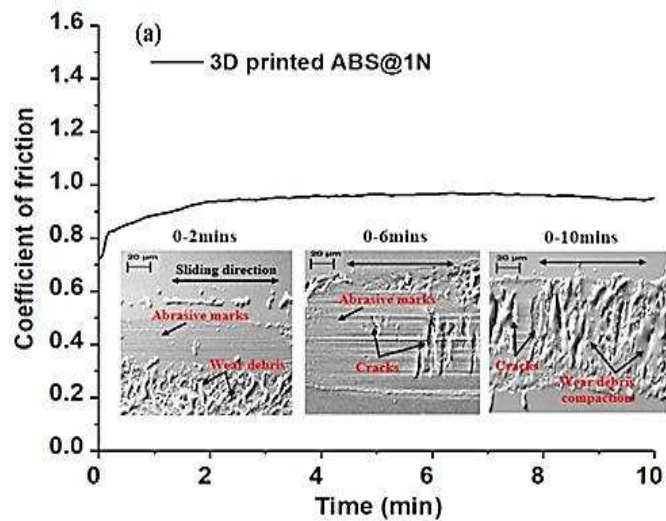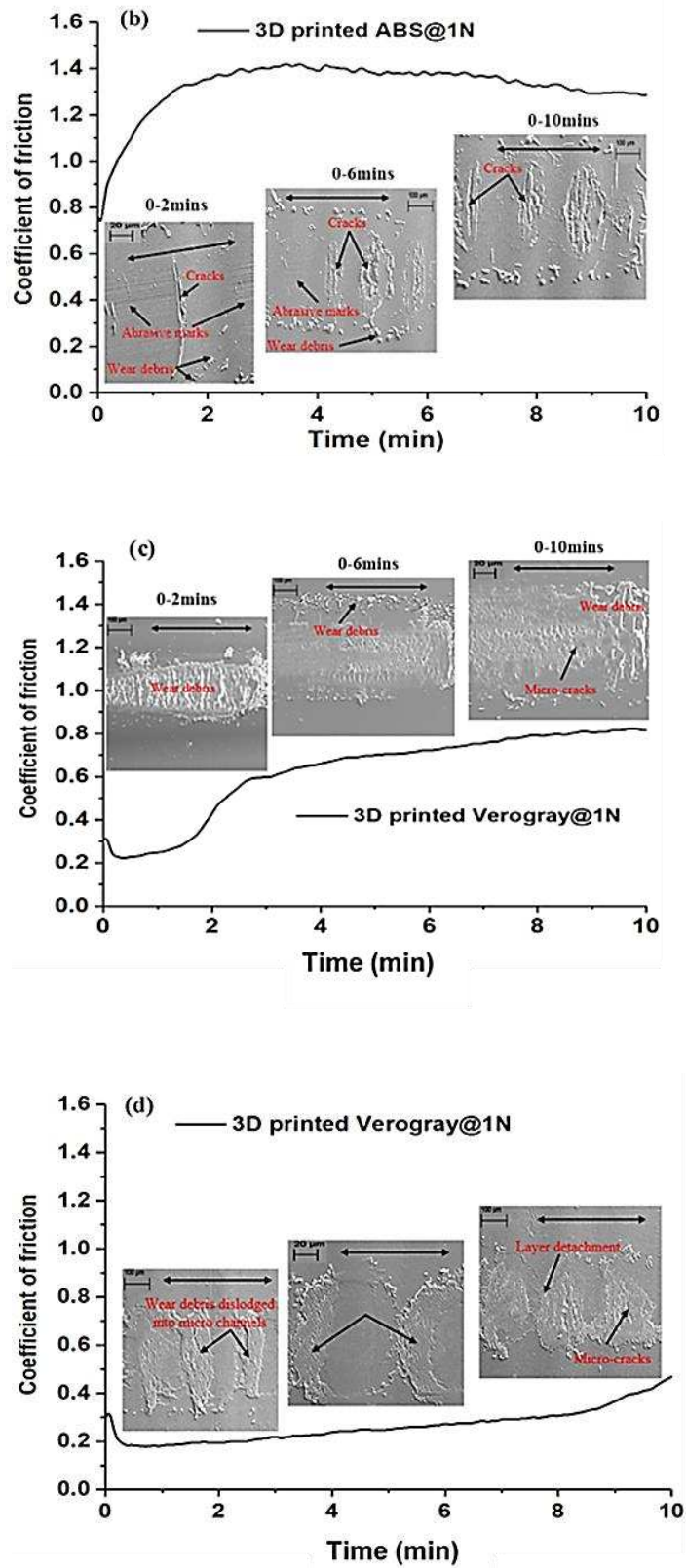
Figure 7. Transient tribological response with varying surface morphology under 1 N load for 3D ABS (a) parallel orientation (b) perpendicular orientation, and Verogray (c) parallel orientation (d) perpendicular orientation.

3.6. Wear Analysis and mechanism

Quantification of wear is typically performed with mass or volume loss measurements. The process of debris generation as a consequence of mechanical and contact fatigue stress encourages surface deformation in the contact area [11]. The wear rates for each sample can be explained by the morphology of the wear presented. From Figure 8, it is observed that the wear resistance of both 3D printed polymers is dependent on the surface orientation at which the sliding occurs. For the 3D ABS, the specific wear rate response (Figure 8 (a)) shows a lower wear rate as the test specimens are orientated perpendicular to the sliding direction. This shows that the use of perpendicular orientation reduces the abrasion of the test specimen surface compared to the parallel orientation. The opposite situation occurs with Verogray, where higher wear rates are observed using perpendicular direction Figure 8 (b). This suggests that the role of material property is crucial in the wear generation process. Interestingly, it is further observed that the directions where higher wear is produced for each specimen cause the lowest friction values, thus supporting the fact that the generation of the third body particles acts as a lubricant during wear. For all applied loads, the surface roughness effect on debris generation is self-evident. Nevertheless, it is observed that the wear generation level is not only dependent on the sliding orientation but also the bulk material resistance to deformation. 3D printed ABS under 1 N load showed better resistance to wear in comparison with Verogray in both print orientations. However, at higher loads of 10 N, the reverse phenomenon is seen for all print orientations where Verogray demonstrates higher resistance to wear than the 3D printed ABS. At 5 N, 3D Verogray perpendicular to the applied load exhibits the highest wear resistance.
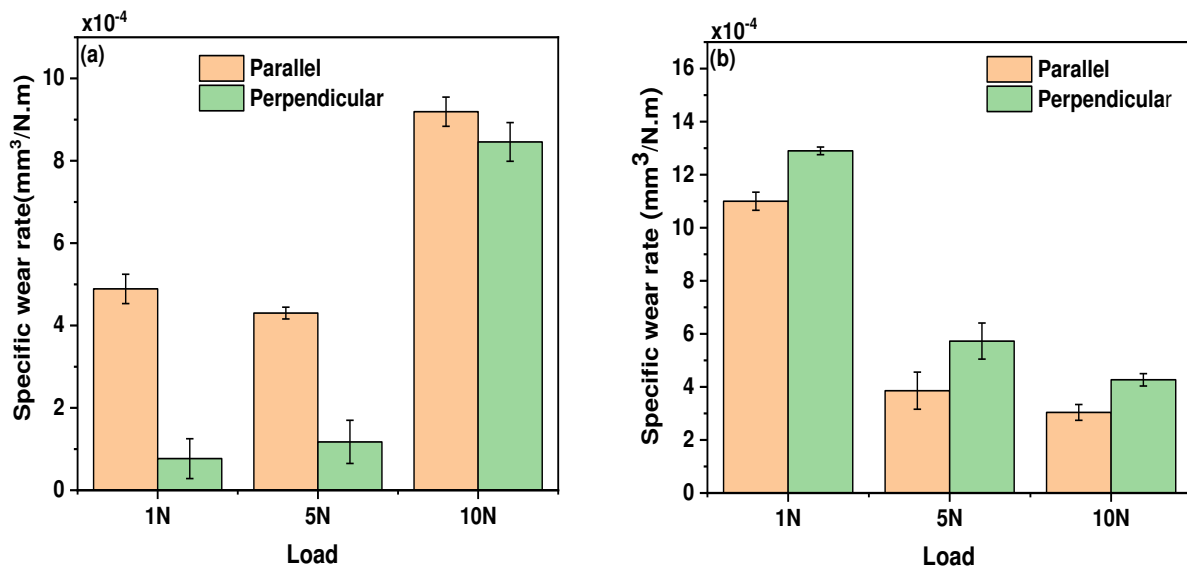

Figure 8. Specific wear rate at 1, 5 and 10 N for (a) 3D ABS (b) Verogray.

Figure 9 and Figure 10 show the SEM micrographs of the wear scars of both test specimens under parallel and perpendicular orientations respectively. It can be observed that at lower loads, the most prominent surface deformation is due to the compaction of the overlapping raster layers. Dawoud et al. [7] observed similar deformation phenomenon with 3D ABS specimen printed with FDM technique under a 35 N load for 60 minutes at a sliding speed of 8.4 m/s. Even though different loads have been applied in both cases, the deformation pattern and the trend observed are very similar. Increasing in the applied load from 1 to 5 N shows a transition from layer

compaction to a mixed regime of both layer detachment and compaction in parallel and perpendicular orientations. As shown in Figure 9 (c) and Figure 10 (c), a further increase in load to 10 N promotes higher surface layer detachment as both abrasive and adhesive damage increases and surfaces are plastically deformed due to high contact load and surface asperity ploughing.

Figure 9. SEM images of 3D ABS showing the influence of polymer print orientation on wear with sliding parallel to the print raster direction at (a) 1 N (b) 5 N (c) 10 N.

Figure 10. SEM images of 3D ABS showing the influence of polymer print orientation on wear with sliding perpendicular to the print raster direction at (a) 1 N (b) 5 N (c) 10 N.
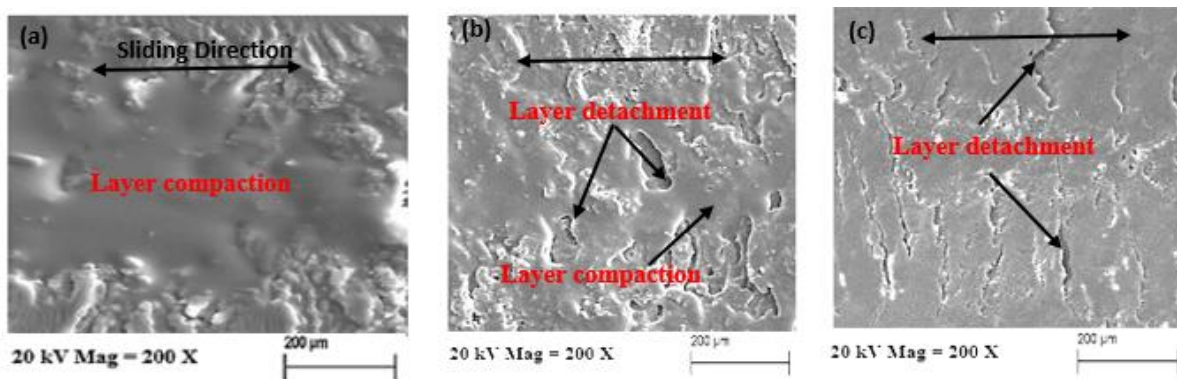
The wear morphology of Verogray is presented in Figure 11 and Figure 12. Figure 11 shows the micrographs of the worn surfaces at 1, 5 and 10 N loads in the parallel orientation. The loss of polymer material in a dry sliding
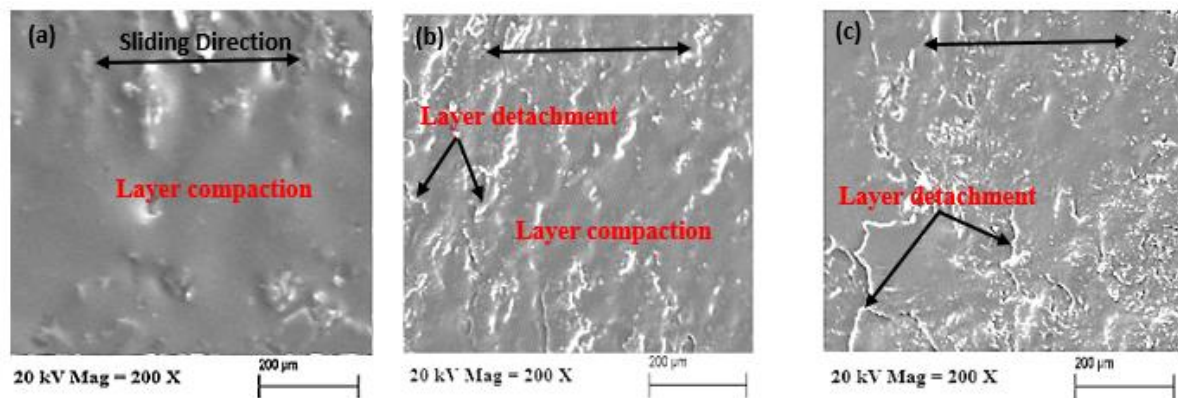

contact between steel and polymer resulting is generally termed friction fatigue [8]. On close inspection of the worn surfaces, wear due to surface fatigue is evident under the different applied loads. However, at higher loads of 10N, the micrograph shown in Figure 11 (c) indicates material removal as a result of adhesive wear. Figure 12 shows the surface micrograph of Verogray post-wear in the perpendicular orientation at 1, 5 and 10 N loads. In Figure 12 (a) and (b), the compression of the polymer surface leading to the development of periodic wave-like deformation and material removal is observed. The abrasive pattern which enhances surface buckling and layer detachment is a common phenomenon known as the Schallamach pattern [39] and is seen under both 1 and 5 N loads. At the higher load of 10 N (Figure 12 (c)), friction fatigue is shown to be dominant, thus leading to the formation of cracks perpendicular to the sliding direction. As Verogray exhibits lower yield strength in

comparison with 3D ABS, the onset of plastic deforming in the initiation and propagation of microcracks during sliding is enhance. This phenomenon is shown to be consistent throughout the different applied loads for the parallel orientation and at 10 N load for the perpendicular orientation.

Figure 11. SEM images of Verogray showing fatigue damage with sliding parallel to the print raster direction at (a) 1N (b) 5 N (c) 10 N.

Figure 12. SEM images of Verogray showing the influence of polymer print orientation on wear with sliding perpendicular to the print raster direction at (a) 1 N (b) 5 N (c) 10 N.
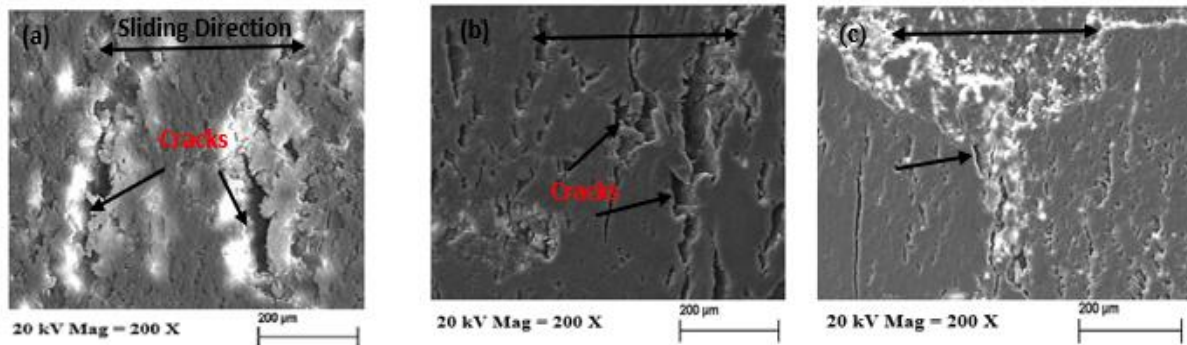
4. Conclusions

3D ABS and Verogray samples were produced using the Polyjet printing technique. Mechanical properties were
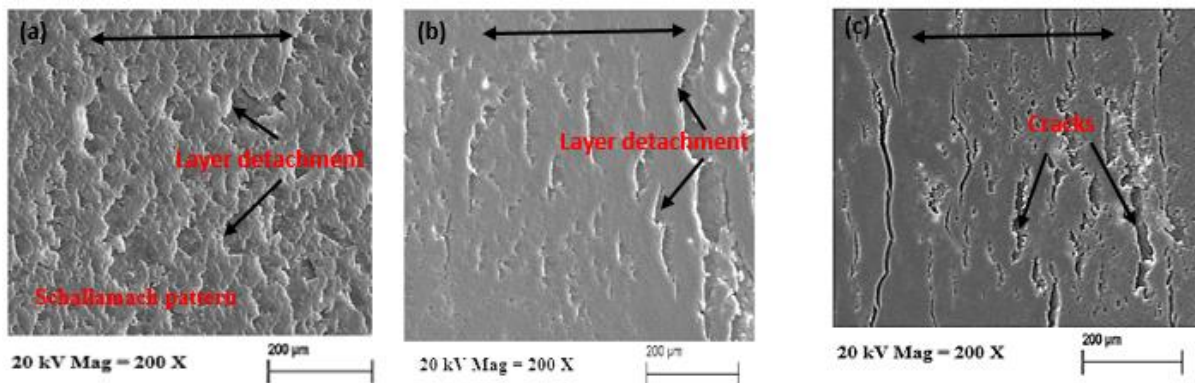
characterised using tensile testing. The individual chemical structure of both test specimen was verified using Fourier Infrared spectroscopy. The tribological response was studied noting the surface roughness of sliding direction relative to the print raster direction at varying loads. The following conclusions can be drawn:

- The frictional performance was shown to be strongly dependent on the surface orientation at 1 N load where surface asperities are seen to play a major role during the reciprocating sliding. However, at higher loads of 5 and 10 N, the bulk mechanical properties affect the coefficient of friction rather to a greater degree than surface roughness.
- Reduced coefficient of friction at low loads is caused by the formation of a low shear tribofilm.
- Wear rates at all loads for 3D ABS was seen to be highest in parallel sliding. However, for Verogray, minimum wear is achieved in the parallel orientation comparatively across the load range.

- Based on the surface morphology of all the worn samples, gross plastic deformation dominates the wear mechanisms in both parallel and perpendicular sliding directions. For the 3D ABS, it was shown that, as the applied load increases, the deformation regime transitions from a predominantly layer compaction to a mixed response characterised by both abrasive wear and layer compaction. Friction fatigue and abrasive wear were both identified as the main characteristic deformation regimes for Verogray.

In future, this work can be extended to investigate the effect of sliding velocity, frequency, micro-scale properties, mechanical interlocking/ micro-welding, temperature and microstructural properties on the tribological behaviour of Polyjet materials.

Acknowledgements

References

[1]   Snyder T, Mick J, Weislogel M, Beyl M, Buchholz A, Molina E, Norris D, Viestenz K and Vu J, "Single-Build Additive Manufacturing of Autonomous Machine," in *NIP & Digital Fabrication Conference*, 2015.

[2]   Stratasys, "Polyjet 3D Printers," Stratasys, [Online]. Available: https://www.stratasys.com/3d-printers/objet1000-plus. [Accessed 1 March 2019].

[3]   Osswald TA and Menges G, "Material Science of Polymers for Engineers," 1995. [Online]. Available: https://www.hanserpublications.com/SampleChapters/9781569905142_9781569905142%20CH-1.pdf. [Accessed 10 June 2019].

[4]   Zhang B, Huang W, Wang J and Wang X, "Comparison of the effect of surface texture on the surface of steel and UHMWPE," *Tribology International,* vol. 65, pp. 138-145, 2013.

[5]   Hong Y, Peng Z, Lee K-H and Chul-Hee L, "Friction and Wear of textured surfaces produced by 3D printing," *Science China Technological Sciences,* vol. 60, pp. 1400-1406, 2017.

[6]   Mohamed OA, Masood SH, Bhowmik JL and Somers AE, "Investigation on the tribological behavior and wear mechanism of parts processed by fused deposition additive manufacturing process," *Journal of Manufacturing Processes,* vol. 29, pp. 149-159, 2017.

[7]   Dawoud M, Taha I and Ebeid SJ, "Effect of processing parameters and graphite content on the tribological behaviour of 3D printed acrylonitrile butadiene styrene," *Mat.-wiss. u. Werkstofftech,* vol. 46, no. 12, pp. 1185-1195, 2015.

[8]   Myshkin N, Petrokovets M and Kovalev A, "Tribology of polymers: Adhesion, friction, wear, and mass-transfer," *Tribology International,* vol. 38, no. 11-12, pp. 910-921, 2005-2006.

[9]   Jacobs O, Jaskulka R, Yan C and Wu W, "On the effect of counterface material and aqueous environment on the sliding wear of various PEEK compounds," *Tribology Letters volume,* vol. 18, p. 359–372, 2005.

[10]   Wang Q, Wang Y, Wang H, Fan N and Yan F, "Experimental investigation on tribological behavior of several polymer materials under reciprocating sliding and fretting wear conditions," *Tribology International,* vol. 104, pp. 73-82, 2016.

[11]   Briscoe B and Sinha S, Polymer Tribology, London: Imperial College Press, 2009.

[12]   Brostow W, Kovačević V, Vrsaljko D and Whitworth J, "Tribology of Polymers and Polymer-based Composites," *Journal of Materials Education,* Vols. 32 (5-6), pp. 273-290, 2010.

[13]   Tahir NAM, Azmi MS, Bin Abdollah MF and Ramli FR, "Tribological properties of 3D-printed pin with internal structure formation under dry sliding condition," in *Proceedings of Mechanical Engineering Research Day 2018*, 2018.

[14]   Sood A, Ohdar R and Mahapatra S, "Parametric appraisal of fused deposition modelling process using the grey Taguchi method," *Journal of Engineering Manufacture,* vol. 224, pp. 135-144, 2009.

[15]   He B, Chen W and Wang Q, "Surface Texture Effect on Friction of a Microtextured Poly(dimethylsiloxane) (PDMS)," *Tribology Letter ,* vol. 31, pp. 187-197, 2008.

[16]   Xi S and Ting N, "Effect of groove textured of fully lubricated sliding with cavitation," *Tribology Internal ,* vol. 44, pp. 2011-2018, 2011.

[17]   Ahn D, Kweon JH, Kwon S, Jungil S and Lee S, "Representation of surface roughness in fused deposition modeling," *Journal of Material Processing Technology,* vol. 209, pp. 5593-5600, 2009.

[18]   Sood AK, Equbal A, Toppo V, Ohdar R and Mahapatra S, "An investigation on sliding wear of FDM built parts," *CIRP Journal of Manufacturing Science and Technology,* vol. 5, pp. 48-54, 2012.

[19]   Dizon J, Espera Jr. A, Chen Q and Advincula RC, "Mechanical characterization of 3D-printed polymers," *Additive Manufacturing,* vol. 20, pp. 44-67, 2018.

[20]   Cazón A, Morer P and Matey L, "PolyJet technology for product prototyping: Tensile strength and surface roughness properties," *Engineering Manufacture,* vol. 228, no. 12, pp. 1664-1675, 2014.

[21]   Stansbury JW and Idacavagec MJ, "3D printing with polymers: Challenges among expanding options and opportunities," *Dental Materials,* vol. 32, no. 1, pp. 54-64, 2016.

[22]   Gaya P, Blanco D, Pelayo F, Noreiga A and Fernández P, "Analysis of Factors Influencing the Mechanical Properties of Flat Polyjet Manufactured Parts," *Pro. Inst. Mech. Eng.B Journal of Engineering Manufacture,* vol. 132, pp. 70-77, 2015.

[23]   Simply Bearings, "simplybearings.co.uk," [Online]. Available: https://simplybearings.co.uk/shop/files/52100.pdf. [Accessed 01 September 2020].

[24]   Bhusha B, Introduction to Tribology, New York: John Wiley, 2013.

[25]   Whitepaper ZT, "Friction and Wear of Polymers," Zeus Industrial Products, Inc, 2005. [Online]. Available: http://www.appstate.edu/~clementsjs/polymerproperties/$p$lastics_$f$riction$5f$w$ear.pdf. [Accessed 1 December 2019].

[26]   Agarwal G, Patnaik A and Sharma RK, "Parametric Optimization and Three-Body Abrasive Wear Behavior of Sic Filled Chopped Glass Fiber Reinforced Epoxy Composites," *International Journal of Composite Materials,* vol. 3, no. 2, pp. 32-38, 2013.

[27]   Arnold C, Monsees D, Hey J and Schweyen R, "Surface Quality of 3D-Printed Models as a Function of Various Printing Parameters," *Materials,* vol. 12, no. 1970, pp. 2-15, 2019.

[28]   Hummel D and Scholl F, Infrared Analysis of Polymers, Resins and Additives: An Atlas of Polymer and Plastic Analysis, München : Weinheim/Carl Hanser Verlag, 1978.

[29]   Stuart B, "Infrared Spectroscopy: Fundamentals and Applications," [Online]. Available: http://www.kinetics.nsc.ru/chichinin/books/spectroscopy/Stuart04.pdf. [Accessed 20 March 2017].

[30]   Griffiths PR and de Haseth JA, Fourier Transform Infrared Spectrometry, New York: Wiley, 1986.

[31]   Larsen TR Ø, "Tribological Studies of Polymer-matrix-composite," Frydenberg a/s, Copenhagen, 2007.

[32]   Archard J, "Elastic deformation and the laws of friction," *Royal Society,* vol. 243, no. 1233, pp. 190-205, 24 December 1957.

[33]   Rees B, "Static friction of bulk polymer over a temperature range," *Research,* vol. 10, pp. 331-338, 1957.

[34]   Kragelskii I, Friction and Wear, Elmsford: Pergamon Press, 1982.

[35]   Quaglini V and Dubini P, "Friction of Polymers Sliding on Smooth Surfaces," *Advances in Tribology,* vol. 2011, pp. 1-8, 2011.

[36]   Rabinowicz E, Friction and Wear of Materials, 2nd ed., Chap.4, New York: Wiley, 1995.

[37]   Fukahori Y and Yamazaki H, "Mechanism of rubber abrasion. Part I: Abrasion pattern formation in natural vulcanizate," *Wear,* vol. 171, pp. 195-202, 1994.

[38]   Boparai K, Singh R and Singh H, "Comparison of tribological behaviour for Nylon6-Al-Al203 and ABS parts fabricated by fused deposition modelling," *Virtual and Physical Prototyping,* vol. 10, no. 2, pp. 59-69, 2015.

[39]   Barquins M, "Sliding friction of rubber and Schallamach waves — A review," *Materials Science and Engineering,* vol. 73, pp. 45-63, 1985.